

# Spin liquid and ferroelectricity close to a quantum critical point in $\text{PbCuTe}_2\text{O}_6$

Ch. Thurn<sup>1\*</sup>, P. Eibisch<sup>1</sup>, A. Ata<sup>1</sup>, U. Tutsch<sup>1</sup>, Y. Saito<sup>1</sup>, S. Hartmann<sup>1</sup>, J. Zimmermann<sup>1</sup>, A. R. N. Hanna<sup>2,3</sup>, A. T. M. N. Islam<sup>3</sup>, S. Chillal<sup>3</sup>, B. Lake<sup>2,3</sup>, B. Wolf<sup>1</sup>, M. Lang<sup>1</sup>

<sup>1</sup>Physikalisches Institut, J.W. Goethe-Universität Frankfurt(M), 60438 Frankfurt, Max-von-Laue-Str.1, Germany

<sup>2</sup>Institut für Festkörperforschung, Technische Universität Berlin, Hardenbergstr. 36, 10623 Berlin, Germany

<sup>3</sup>Helmholtz-Zentrum Berlin für Materialien und Energie, Hahn-Meitner Platz 1, 14109 Berlin, Germany

\*e-mail: [Thurn@Physik.uni-frankfurt.de](mailto:Thurn@Physik.uni-frankfurt.de)

**Geometrical frustration among interacting spins combined with strong quantum fluctuations destabilize long-range magnetic order in favor of more exotic states such as spin liquids. By following this guiding principle, a number of spin liquid candidate systems were identified in quasi-two-dimensional (quasi-2D) systems. For 3D, however, the situation is less favorable as quantum fluctuations are reduced and competing states become more relevant. Here we report a comprehensive study of thermodynamic, magnetic and dielectric properties on single crystalline and pressed-powder samples of  $\text{PbCuTe}_2\text{O}_6$ , a candidate material for a 3D frustrated quantum spin liquid<sup>1-3</sup> featuring a hyperkagome lattice. Whereas the low-temperature properties of the powder samples are consistent with the recently proposed quantum spin liquid state<sup>1-3</sup>, an even more exotic behaviour is revealed for the single crystals. These crystals show ferroelectric order at  $T_{\text{FE}} \approx 1$  K, accompanied by strong lattice distortions, and a modified magnetic response – still consistent with a quantum spin liquid – but with clear indications for quantum critical behaviour.**

Competing interactions combined with strong quantum fluctuations are considered a major guiding principle for the realization of a quantum spin liquid. This long sought state of matter is characterized by exciting properties such as macroscopic entanglement and fractionalized excitations, see refs. [4-8] for recent reviews. As quantum fluctuations are enhanced for low spin values and low lattice coordination, most efforts have been devoted to low-dimensional (low-D) quantum spin ( $S = 1/2$ ) antiferromagnets, with prominent examples including the 2D kagome system Herbertsmithite<sup>9,10</sup> and some layered triangular-lattice charge-transfer salts<sup>11-13</sup>. For 3D lattices, the search has focused on materials where the spins reside on a

pyrochlore<sup>14,15</sup> or hyperkagome lattice<sup>16</sup>, a 3D network of corner-sharing triangles. As in 3D competing ground states are expected to become more relevant, perturbations from purely Heisenberg spin scenarios due to, e.g., Dzyaloshinskii-Moriya interaction<sup>17,18</sup> or spin-orbit coupling<sup>19</sup> gain in importance and may eventually govern the materials' ground state<sup>4</sup>. This raises the question about the stability of a quantum spin liquid phase in 3D. In fact, for Na<sub>4</sub>Ir<sub>3</sub>O<sub>8</sub>, a 3D effective  $S = 1/2$  spin liquid candidate system with a hyperkagome lattice<sup>16</sup>, evidence was reported for a nearby quantum critical point<sup>20</sup> – a  $T = 0$  instability to some nearby (possibly magnetically) ordered state. More recently, PbCuTe<sub>2</sub>O<sub>6</sub> has attracted considerable interest as another 3D quantum spin liquid candidate system featuring a highly-connected hyperkagome lattice<sup>1-3</sup>, where  $S = 1/2$  Cu<sup>2+</sup> spins are coupled by isotropic antiferromagnetic interactions. According to recent magnetic studies, mainly on pressed-powder samples<sup>1-3</sup>, this system lacks long-range magnetic order down to 0.02 K<sup>2</sup> and shows diffuse continua in the magnetic spectrum<sup>3</sup> consistent with fractional spinon excitations. Puzzling issues relate to the appearance of small anomalies in the powder samples around 1 K of unknown origin<sup>1-3</sup> and signs of a phase transition around this temperature in first-generation single crystals<sup>3</sup>.

In the present work, we present a comprehensive study of thermodynamic, magnetic and dielectric properties of PbCuTe<sub>2</sub>O<sub>6</sub>, with special focus lying on its low-temperature state. To this end, we have investigated several single crystals and compare the results with data on pressed-powder samples. The salient results of our study are (i) the observation of a phase transition in single crystalline material around 1 K into a ferroelectrically-ordered state, which is accompanied by strong lattice distortions. (ii) This phase transition and the state at  $T \leq 1$  K is characterized by a finite

magnetic susceptibility without any indication for long-range magnetic order consistent with a gapless quantum spin liquid state. (iii) The bulk ferroelectric transition and its accompanying lattice distortions are absent in the powder samples. (iv) For these powder samples, the ratio  $\alpha/C$ , with  $\alpha$  the thermal expansion coefficient and  $C$  the specific heat, probing the thermal Grüneisen parameter  $\Gamma_p$ , is independent of temperature for  $T \leq 1.6$  K. In contrast, a corresponding uniaxial Grüneisen parameter for the single crystal shows a strong increase for  $T \rightarrow 0$ , potentially indicating quantum critical behaviour. In fact, clear evidence for a nearby field-sensitive quantum critical point is observed in the magnetic Grüneisen parameter  $\Gamma_B$ , yielding a divergence for  $T \rightarrow 0$ .

$\text{PbCuTe}_2\text{O}_6$  crystallizes in a non-centrosymmetric cubic structure with space group  $P4_132$  (No. 213). According to density functional theory calculations<sup>3</sup> based on room-temperature structural data, the magnetic lattice can be described by isolated equilateral  $S = 1/2$  triangles with nearest-neighbour interaction  $J_1 = 1.13$  meV, which are coupled via the second-nearest neighbour interaction  $J_2 = 1.07$  meV into a hyperkagome lattice. The weaker third- and fourth-nearest neighbour interactions  $J_3 = 0.59$  meV and  $J_4 = 0.12$  meV couple the spins into chains. Another unique feature of  $\text{PbCuTe}_2\text{O}_6$ , which has been largely ignored until now, relates to its dielectric degrees of freedom<sup>21</sup>. The material contains polar building blocks originating from the free electron pairs (lone pairs) of the  $\text{Te}^{4+}$  ions in the oxotellurate tetrahedrons and the asymmetrically coordinated  $\text{Pb}^{2+}$  ions. These characteristics together with the non-centrosymmetric structure imply the possibility of ferroelectric order interacting with the strongly frustrated quantum spin system. In fact, a magneto-dielectric effect was

observed in  $\text{SrCuTe}_2\text{O}_6$  (ref. 22) which is isostructural to  $\text{PbCuTe}_2\text{O}_6$  but features a magnetic network with predominantly 1D character.

Measurements were performed on single crystals (sc) from 4 different batches grown by utilizing two different techniques (see Methods and ref. 23), and pressed-powder (pd) samples from the same batch prepared as described in ref. 3. In what follows, the samples will be specified by giving their batch number followed by an alphabetic character to distinguish different samples from the same batch.

Figure 1 shows the results of the specific heat,  $C$ , measured on single crystal sc #5(b). The data reveal a pronounced  $\lambda$ -shape phase transition anomaly around 1 K, signaling a second-order phase transition, on top of a broad maximum. The figure also includes data for a pressed-powder sample pd #I(b) showing a distinctly different behaviour. Here we find the broad maximum in  $C(T)$  centered around 1.4 K, followed by a smooth reduction upon further cooling similar to previous reports on powder material<sup>1-3</sup>. As also revealed in these studies, we observe signatures for a tiny feature around 1 K and a  $C(T) \propto T^n$  dependence at temperatures  $T \leq 0.4$  K with  $n \approx 2$ .

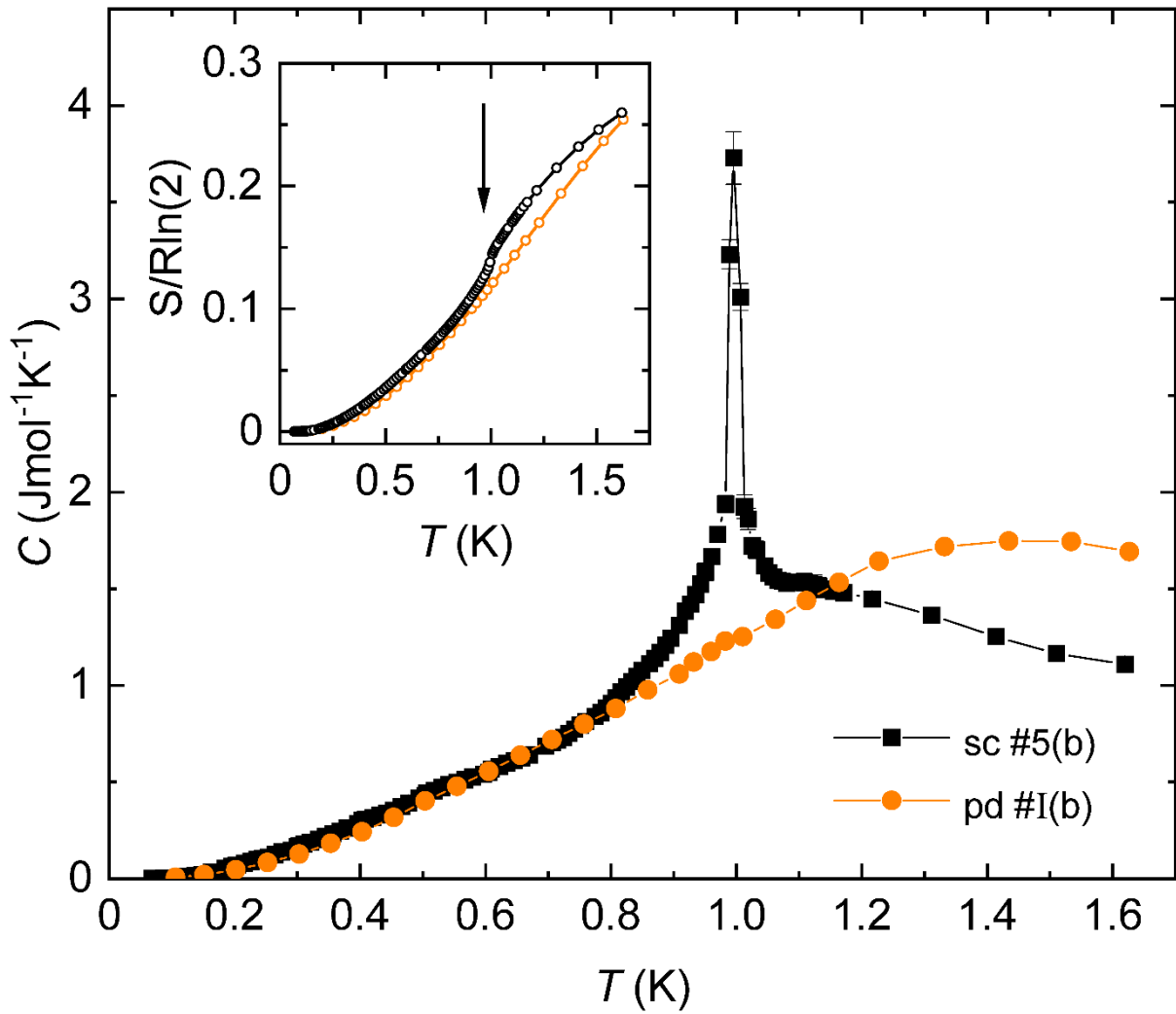


**Figure 1** Temperature dependence of the specific heat of  $\text{PbCuTe}_2\text{O}_6$ . Specific heat of single crystal sc #5(b) (black squares) and a pressed-powder sample pd #1(b) (orange spheres). Very similar results to those on sc #5(b) were obtained on a second single crystal #1(b) studied in this experiment, which was grown using a different technique, see Methods and supplementary information (SI). The data were corrected for nuclear contributions, see SI. The inset shows the entropy in units of  $R\ln 2$  for both samples using the same colour code. The arrow marks the position of the phase transition anomaly in  $C(T)$ . The entropy release associated with the phase transition over a narrow temperature window of about 0.2 K amounts to a few percent of  $R\ln 2$ .

More insight into the nature of the phase transition in the single crystalline material can be obtained by studying the elastic properties via thermal expansion measurements, cf. Fig. 2. In the inset of Fig. 2, we show data of the relative length changes,  $\Delta L_i(T)/L_i$ , for sc #1(a) measured along two different directions. Based on structure determination at room temperature, we refer to these directions as  $i = [100]$  and  $[1-10]$ . For the data at higher temperatures down to about 1.7 K, we find a smooth isotropic reduction of  $\Delta L_i(T)/L_i$  with decreasing temperature, consistent with a cubic structure. However, on further cooling the thermal contraction becomes increasingly stronger and develops a pronounced anisotropy, indicating deviations from cubic symmetry at low temperatures. At around 1 K we find a sharp break in the slope in  $\Delta L_i(T)/L_i$  along both directions, consistent with a second-order phase transition. We stress that the evolution of a non-isotropic lattice strain from a cubic high-temperature state implies the formation of structural domains. As a result, the  $\Delta L_i(T)/L_i$  data for  $T \leq 1.7$  K in Fig. 2 could potentially be affected by the material's domain structure. In general, the formation of domains can be influenced by the application of uniaxial pressure to the crystal in its high-temperature phase. This is actually the case in our thermal expansion measurements along the measuring direction, where uniaxial pressure of order 0.01 – 5 MPa is applied, depending on the sample geometry and the chosen starting capacitance, see supplementary information (SI) and ref. 24. In the main panel of Fig. 2 we show the coefficient of thermal expansion  $\alpha_i(T) = 1/L_i \cdot d(\Delta L_i(T))/dT$  for single crystal sc #5(c) along the  $[110]$  direction. Since in this experiment a rather high uniaxial pressure of about  $(6.5 \pm 1.3)$  MPa was realized, we believe that these  $\alpha_{[110]}$  data represent a preferential domain orientation if not a mono-domain structure, see SI. Therefore, we confine the discussion of the temperature dependence to these  $\alpha_{[110]}$  data. Upon cooling,  $\alpha_{[110]}$  shows an extraordinarily strong

increase followed by a sharp negative phase transition anomaly slightly below 1 K, and a second maximum around 0.5 K. However, assuming that the phase transition anomaly in  $\alpha(T)$  has the same narrow  $\lambda$  shape as the one observed in  $C(T)$  (cf. Fig. 1) suggests another interpretation: there is only a single huge maximum in  $\alpha_{[110]}$  centered around  $(0.75 \pm 0.1)$  K to which a negative  $\lambda$ -shape phase transition anomaly around 1 K is superimposed. Figure 2 also shows thermal expansion data taken on the pressed-powder sample pd #I(a). Whereas the  $\Delta L(T)/L$  data for the powder match with the data for the single crystal for  $T > 1.6$  K, (see inset of Fig. 2) they deviate at lower temperatures: instead of the strong contraction observed for the single crystal on approaching the phase transition, the powder sample shows a rather smooth behaviour with  $\Delta L(T)/L$  gradually levelling off upon cooling. The corresponding  $\alpha(T)$  data for the powder sample shown in the main panel of Fig. 2 reveal a broad maximum around 1.4 K followed by a smooth variation  $\alpha(T) \propto T^n$  with  $n \approx 2$  for  $T \leq 0.4$  K.

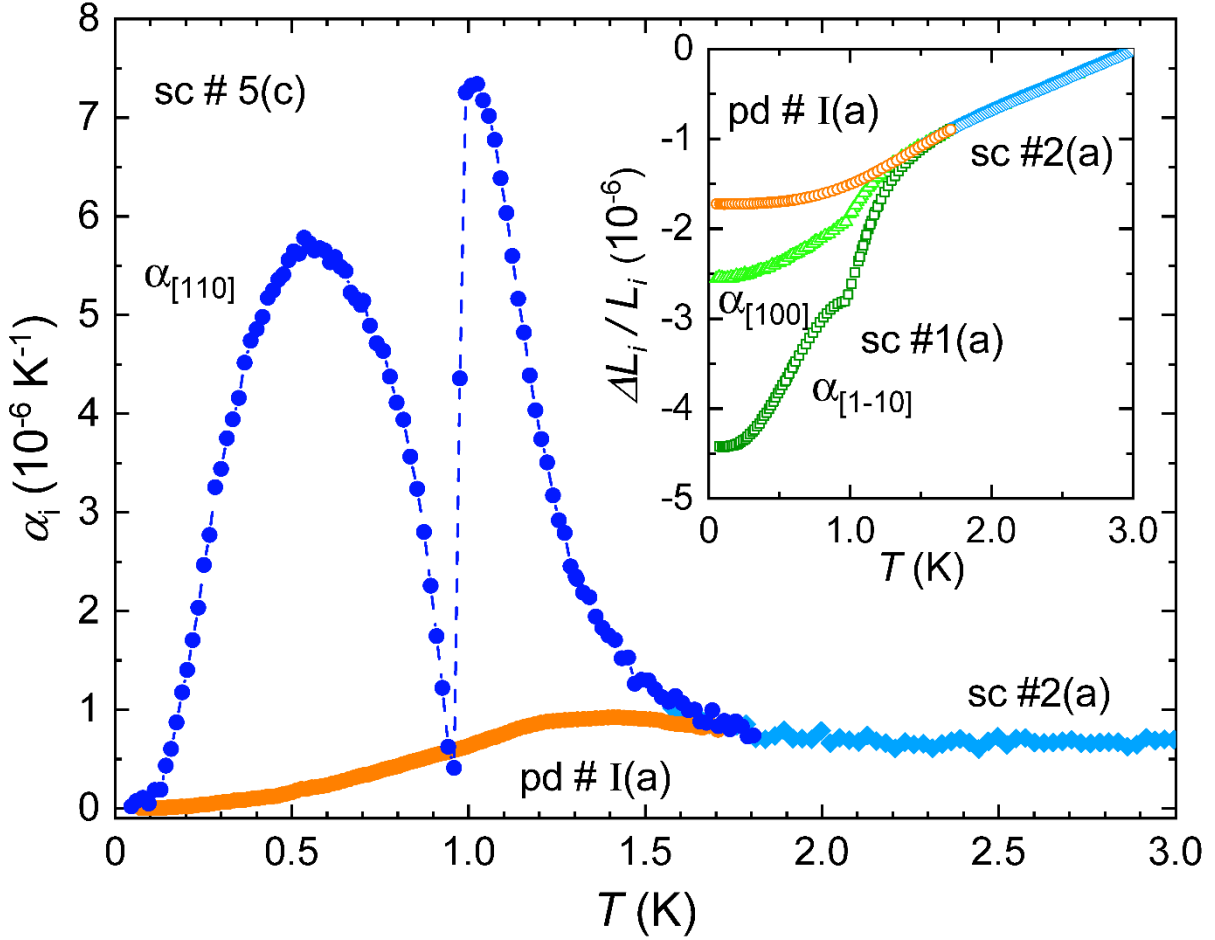


**Figure 2** Temperature dependence of the coefficient of thermal expansion of  $\text{PbCuTe}_2\text{O}_6$ . Thermal expansion coefficient  $\alpha$  for single crystal sc #5(c) (dark blue spheres) and sc #2 (light blue diamonds for  $T \geq 1.6$  K), both measured along the [110] direction, together with data for the pressed-powder sample pd #I(a) (orange spheres). Broken line serves as a guide to the eyes. The inset shows relative length changes  $\Delta L_i(T)/L_i$  for sc #1(a), measured along [100] (light green triangles) and [1-10] (dark green squares), sc #2 (light blue diamonds) for  $T \geq 1.5$  K, and for the powder sample pd #I(a) (orange spheres). The large effect in  $\Delta L_i(T)/L_i$  along the [110] direction is consistent with a strong decrease observed in the longitudinal elastic constant  $c_{L[110]}$  upon cooling, see figure S7 in SI.

Given the material's non-centrosymmetric structure and its polar building blocks, comprising two subsystems of stereochemically active lone pairs associated with the  $\text{Te}^{4+}$  and  $\text{Pb}^{2+}$  ions, the observation of a lattice distortion suggests an involvement of the electric degrees of freedom. To probe the dielectric response, measurements of the dielectric constants were performed on single crystals #1(a), #4 and #5(b) for temperatures  $T \leq 1.3$  K. In Fig. 3 we show exemplarily the results of the normalized dielectric constant  $\varepsilon'$  for sc #5(b). The data reveal an enhanced background dielectric constant of  $\varepsilon'_b \approx 18$  in the temperature range investigated and a well-pronounced peak centered at 0.97 K, signaling a ferroelectric transition at  $T_{\text{FE}} = 0.97$  K. This assignment is further corroborated by a Curie-Weiss-like behaviour on approaching the maximum in  $\varepsilon'$  from both sides, see inset (A) of Fig. 3. In the inset (B) of Fig. 3 we show the frequency dependence of the dielectric anomaly around 1 K. The measurements, covering approximately two decades in frequency, reveal a distinct suppression of the peak with increasing frequency whereas the position of the peak remains essentially unchanged. This behaviour is typical for an order-disorder-type ferroelectric transition<sup>26,28</sup> where electric dipoles that are disordered at high temperature order with a net overall polarization below  $T_{\text{FE}}$ . In contrast for the pressed-powder sample pd #I(b) we find only a tiny anomaly in  $\varepsilon'$  around 1 K, see Fig. 3. This observation together with the smooth variation of  $\Delta L(T)/L$  for  $T \leq 1.6$  K for the powder sample, reflecting the absence of a lattice distortion, indicate that there is no bulk ferroelectric transition in the pressed-powder sample.

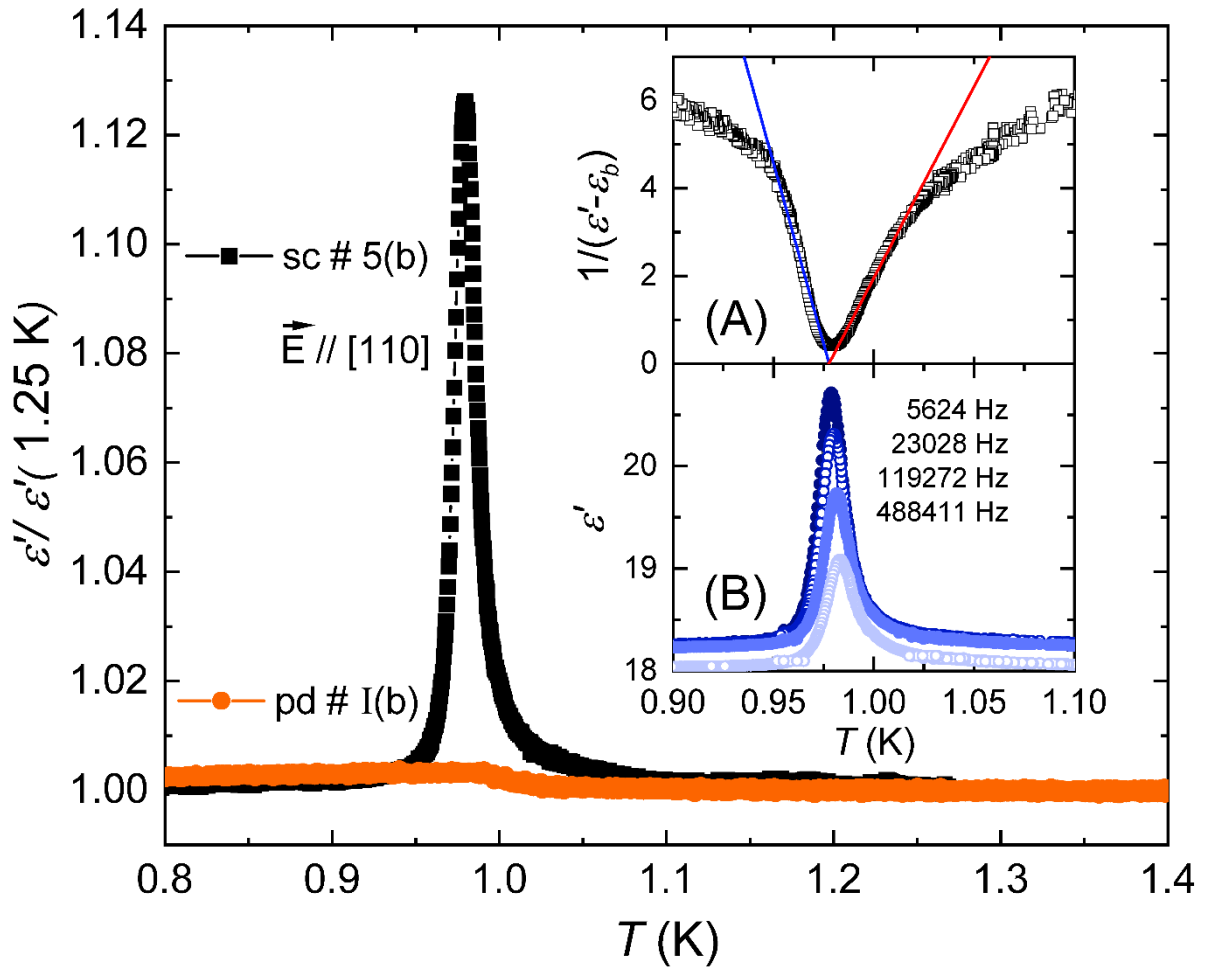


**Figure 3** Temperature dependence of the dielectric constant of  $\text{PbCuTe}_2\text{O}_6$ .

Dielectric constant of single crystal sc #5(b) (black squares), with the electric field  $\mathbf{E}$  applied along the [110] direction, and a pressed-powder sample pd #I(b) (orange spheres). Similar measurements on the single crystals #1(a) and #4 reveal essentially the same results albeit with a somewhat reduced peak height, see SI. The inset gives details of the data for sc #5(b) in a narrow temperature range around 1 K. Inset (A), showing  $1/(\epsilon' - \epsilon'_b)$  vs.  $T$ , reflects a Curie-Weiss-like behaviour on approaching the maximum in  $\epsilon'$  from both sides. The slopes of the linear regimes differ by a factor of about -1.9. This factor is very close to -2, expected for a mean-field second-order ferroelectric transition<sup>25</sup>, but strongly departs from -8 seen at first-order ferroelectric

transitions<sup>26,27</sup>. The lower inset (B) shows  $\epsilon'$  vs.  $T$  for varying frequencies as indicated in the figure. The small shift of the background dielectric constant  $\epsilon'_b$ , visible for the data at highest frequency, indicates some contribution from extrinsic factors.

The different dielectric and lattice properties observed here for the pressed-powder material as opposed to the single crystals, can be rationalized by considering that the powder samples studied here and in the literature<sup>1-3</sup> were all prepared by a solid-state reaction method where the material is subject to multiple grinding processes interrupted by special heat treatments. Correspondingly, these samples constitute a more or less homogeneous collection of grains with some distribution of grain sizes, which may vary from sample to sample and the heat treatment applied. Our finding of a ferroelectric transition in the single crystalline material and the suppression of this transition in the pressed-powder samples is consistent with results on grain-size effects in ferroelectric ceramics (see, e.g., refs. 29-31), yielding a critical grain size below which the transition disappears.

The drastic reduction of the anomaly in  $\epsilon'$  around 1 K for the powder sample, together with the smooth behaviour in the thermal expansion and specific heat (Fig. 1 and Fig. 2) are fully consistent with the absence of a bulk ferroelectric transition and the accompanying lattice distortion in the powder sample. At the same time, as demonstrated by various advanced magnetic measurements<sup>2,3</sup>, these powder samples lack long-range magnetic order down to temperatures as low as 0.02 K, indicating that in the non-distorted cubic low-temperature state of  $\text{PbCuTe}_2\text{O}_6$ , the frustration of the

magnetic network is strong enough to suppress long-range ordering consistent with the formation of a quantum spin liquid state. This raises the question to what extent the magnetic lattice and thus the degree of frustration is altered by the lattice distortions revealed in single crystalline material. In this context it is interesting to note that the broad maximum in the low-temperature specific heat, a feature which is considered a hallmark of strongly frustrated spin systems<sup>1,16,20,32,33</sup>, shows a considerable shift from  $T_{\max} \approx 1.4$  K for the powder sample to below 1 K for the single crystalline material. It is tempting to assign this shift to strain-induced alterations of the exchange coupling constants in the frustrated spin system in the single crystals. This is consistent with results for the magnetization  $M(T)$  derived from ac-susceptibility measurements on single crystal #5(b) (see inset to Fig. 4), still lacking any indication for long-range order for  $T \geq 0.1$  K, which reveal a small reduction of  $M(T)$  with decreasing temperatures below about 0.8 K. In contrast, for powder material a slight increase was observed for  $M(T)$  on cooling below 1 K<sup>2</sup>.

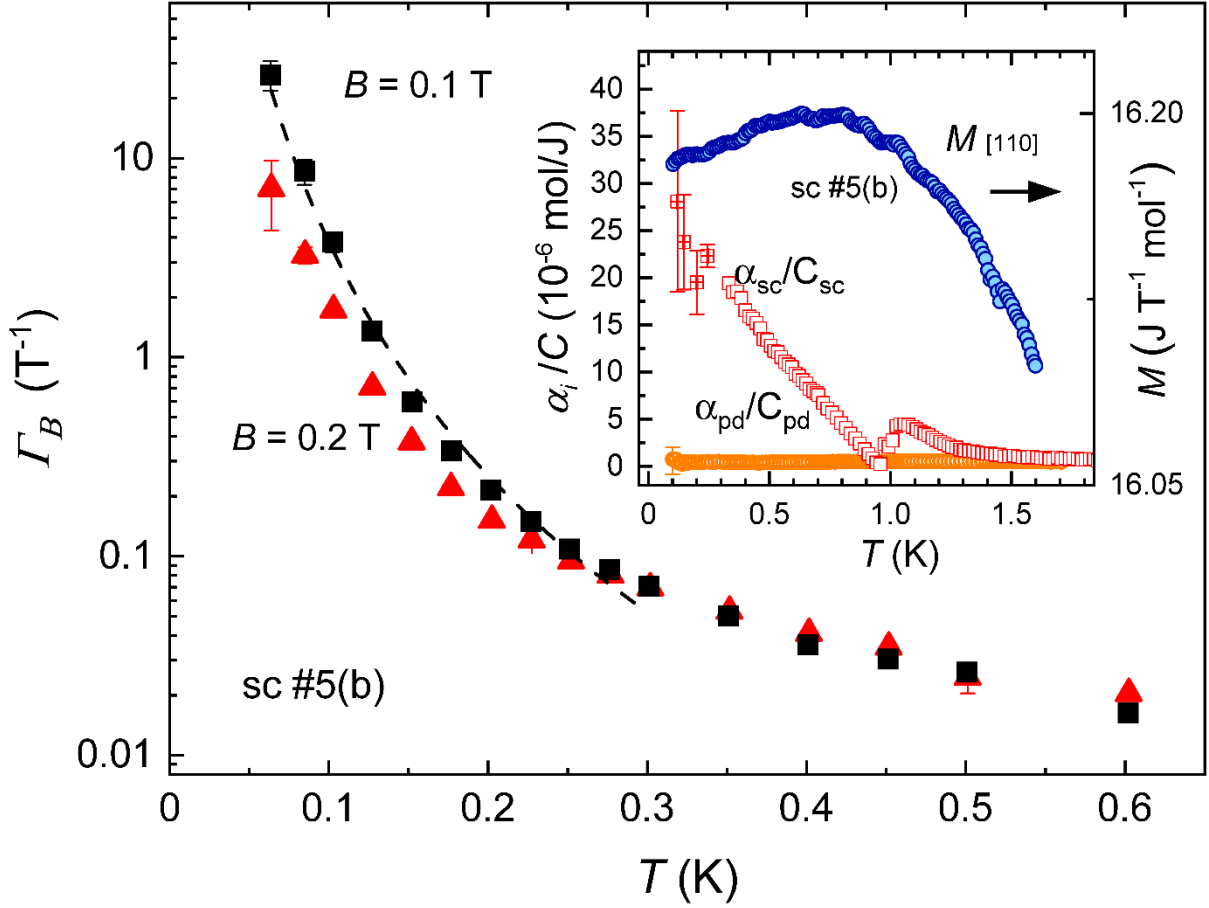


**Figure 4 Temperature dependence of the magnetic Grüneisen parameter.** Magnetic Grüneisen parameter  $\Gamma_B = 1/T \cdot (\partial T / \partial B)_S$  as a function of temperature for  $\text{PbCuTe}_2\text{O}_6$  single crystal #5(b) in a semi-logarithmic representation. The data represent the electronic contribution  $\Gamma_{B,e}$  which is obtained from the measured  $\Gamma_B$  after correcting for nuclear contributions, see SI. Data were taken by applying small field ramps of  $\Delta B = \pm 0.03$  T on top of a dc field of  $B = 0.1$  T (black squares) and  $0.2$  T (red triangles) applied along [110], see SI and ref. 35 for details on the technique applied. A minimum dc field of  $0.1$  T was used to avoid issues associated with remnant fields of the magnet. Broken line shows a fit  $T^m$  with  $m = 3.9$  for  $T \leq 0.3$  K. The inset (left ordinate) shows the ratio  $\alpha_{sc}/C_{sc} = \alpha_{[110]}/C_{sc}$  for single crystal #5 (open red squares)

and  $\alpha_{pd}/C_{pd}$  for the pressed-powder sample pd #I (open orange spheres) both measured at  $B = 0$ . Since for  $T \leq 1$  K the lattice contributions to  $\alpha$  and  $C$  are very small, their influence can be neglected in discussing the critical behaviour of the Grüneisen ratio. The inset also shows results for the magnetization (right ordinate) per mole in a field of  $B = 0.1$  T along the [110] direction of sc #5(b) obtained by ac-susceptibility measurements. The data, which lack any indications for long-range magnetic order, reveal small differences to the  $M(T)$  behaviour found for powder material<sup>2</sup>. Despite these small differences, inelastic neutron scattering<sup>3</sup> on a single crystal sample reveal continuous magnetic excitations similar to those observed for the pressed powder, consistent with deconfined spinon excitations in a quantum spin liquid.

Another even more pronounced difference in the materials' low-temperature magnetic/electronic state becomes apparent by studying the ratio  $\alpha_{[110]}/C$  for sc #5, a quantity which is proportional to the uniaxial thermal Grüneisen parameter  $\Gamma_{p[110]}$  (see ref. 34) and compare this to  $\alpha/C$  for the pressed-powder sample pd #I, cf. inset of Fig. 4. The figure reveals a practically temperature-independent ratio for the pressed-powder sample in the temperature range investigated. This is consistent with the notion that the low-energy excitation spectrum in the powder material is governed by a single energy scale, the pressure dependence of which is probed by  $\Gamma_p$ . We link this energy scale to the maximum in  $\alpha$  and  $C$  at  $T_{max}$  around 1.4 K which reflects magnetic correlations in the strongly frustrated hyperkagome lattice. In contrast, for the single crystal, we find a distinctly different behaviour. Whereas the ratio at higher

temperatures lies close to the value for the powder material, it shows a distinctly different temperature dependence upon cooling. Of particular interest is the behaviour at lowest temperatures where the influence of the phase transition anomalies in  $\alpha_{[110]}$  and  $C$  around  $T_{FE} \approx 1$  K is expected to be small, suggesting it is related to the magnetic sector. In fact the data reveal a growing ratio  $\alpha_{[110]}/C$  upon cooling for low temperatures. However, in light of the substantial error bars involved, the data do not allow to make a definite statement on the asymptotic behaviour, especially whether or not this ratio diverges for  $T \rightarrow 0$ . In general, a diverging Grüneisen ratio  $\Gamma_p = 1/T \cdot (\partial T / \partial p)_S$ , measuring temperature contours at constant entropy  $S$ , is considered a clear signature of a nearby pressure ( $p$ )-sensitive quantum critical point<sup>34</sup>. It results from the accumulation of entropy close to the quantum critical point.

As an alternative approach for probing potential quantum critical behaviour associated with the system's magnetic degrees of freedom, we performed measurements of the magnetic Grüneisen parameter  $\Gamma_B = 1/T \cdot (\partial T / \partial B)_S$ <sup>34</sup>. In fact, as shown in the main panel of Fig. 4, the data reveal a diverging  $\Gamma_B$  on cooling over about one decade in temperature down to 0.06 K with an asymptotic behaviour following a  $\Gamma_B \propto T^m$  dependence with  $m \approx 3.9$ . Note that an independent determination of  $\Gamma_B$  is provided by using the identity  $\Gamma_B = -(dM/dT)/C$ <sup>34</sup>. In fact, based on the  $M(T)$  data (inset of Fig. 4) and  $C(T)$  data (Fig. 1), we obtain an almost identical behaviour for  $\Gamma_B(T)$  within the experimental uncertainty, see Fig. S3 in SI, that is, a divergence for  $T \rightarrow 0$ . From these observations, we conclude that single crystalline  $\text{PbCuTe}_2\text{O}_6$  for  $T \rightarrow 0$  approaches a quantum critical point which is sensitive to magnetic fields. This is consistent with results taken on mildly increasing the magnetic field to  $B = 0.2$  T (Fig. 4), and the variation of  $\Gamma_B$  with field measured at  $T = 0.15$  K (see SI), yielding a

suppression of  $\Gamma_B$  following a  $\Gamma_B = -A/(B - B_c)$  dependence with  $A = 0.058 \pm 0.005$  and  $B_c \approx 0$ . According to ref. 34 this behaviour is expected for a quantum paramagnetic state, that is, a non-critical spin-correlated state. This raises the question about the origin of the quantum critical behaviour that gives rise to the divergence in  $\Gamma_B(T)$  at small fields. In light of the strong response revealed for the uniaxial Grüneisen parameter along the [110] direction, we associate the quantum critical behaviour to an instability of the quantum spin liquid against uniaxial pressure  $p_{[110]}$  and the associated lattice distortions. It remains to be shown by future experiments on mono-domain single crystals whether or not there are divergences in the uniaxial Grüneisen parameters also along the orthogonal [1-10] and [001] directions. Remarkably, an anisotropic thermal expansion response with quantum critical behavior only along one direction was observed for the heavy fermion metal CeRhSn<sup>36</sup> featuring a frustrated 2D kagome lattice.

In conclusion, comprehensive investigations on PbCuTe<sub>2</sub>O<sub>6</sub> including thermodynamic, magnetic and dielectric probes, reveal markedly different behaviour for single crystalline material as compared to pressed-powder samples: whereas the low-temperature properties of the powder material are consistent with the recently proposed gapless quantum spin liquid state, an even more exotic behaviour is observed for the single crystals. Here, we find a ferroelectric transition at  $T_{FE} \approx 1$  K, accompanied by pronounced lattice distortions, and modified magnetic signatures - still consistent with a quantum spin liquid - but with clear indications for quantum critical behaviour. These findings call for low-temperature structural investigations as key input for determining the modified exchange interactions for this material. In the absence of such low- $T$  structural information, we speculate that the lattice distortions

in single crystalline material are likely to deform the frustrated hyperkagome lattice in a way that drives the system close to a quantum critical point. Based on the trend revealed by comparing the maximum in the specific heat at  $T_{\max}$  for various frustrated antiferromagnets<sup>16</sup>, we are inclined to assign the reduction of  $T_{\max}$  from 1.4 K for the powder to below 1 K for the single crystals to an increase in the degree of frustration, thereby driving the system quantum critical. It is interesting to note that quantum critical behaviour, assigned to geometrical frustration, has been observed also in other materials where a 3D frustrated spin system interacts with charge degrees of freedom such as in the Kondo lattice  $\text{Pr}_2\text{Ir}_2\text{O}_7$  (ref. 37) or the valence fluctuator  $\beta\text{-YbAlB}_4$  (ref. 38).

In contrast to these systems,  $\text{PbCuTe}_2\text{O}_6$  features a pure spin system which is devoid of effects related to spin-orbit interactions, crystalline electric fields or Kondo-type interaction with delocalized charges. Thus single crystalline  $\text{PbCuTe}_2\text{O}_6$  offers the possibility for exploring quantum criticality resulting from a strongly frustrated hyperkagome spin system interacting with ferroelectricity – a novel scenario holding promise for interesting physics. Especially, through comparison with the non-critical behaviour of the undistorted low- $T$  state realized in the pressed-powder samples of  $\text{PbCuTe}_2\text{O}_6$ , one may expect to find interesting magneto-electric coupling effects mediated by the lattice deformations, indications of which are actually observed in measurements under magnetic fields and will be published independently.

## Methods

**Samples investigated.** Single crystals of  $\text{PbCuTe}_2\text{O}_6$  were grown by utilizing two different techniques: a travelling solvent floating zone (TSFZ) method for sc #1, sc #2, and sc #4, and a top-seeded solution growth (TSSG) technique for sc #5. According to the structural characterization in ref. [23], the single crystals grown by the TSFZ technique may contain foreign phases with a volume fraction of 6 % at maximum. In contrast, no foreign phase could be detected in these measurements for the crystals grown by using the TSSG method.

**Thermal expansion.** Thermal expansion experiments were performed by using a homemade capacitive dilatometer following the design discussed in ref. 39. In this technique, relative length changes  $\Delta L(T)/L$  are measured with  $\Delta L(T) = L(T) - L(T_0)$  and  $T_0$  the starting temperature of the experiment. Measurements were performed at temperatures  $0.05 \text{ K} \leq T \leq 2 \text{ K}$ , using a bottom bottom-loading  $^3\text{He}$ - $^4\text{He}$  dilution refrigerator and for  $1.5 \text{ K} \leq T \leq 200 \text{ K}$ , using a  $^4\text{He}$  bath cryostat.

**Specific heat.** The specific heat measurements were carried out by employing both a homemade relaxation calorimeter as well as a homemade continuous-heating-type calorimeter both of which were attached to bottom-loading  $^3\text{He}$ - $^4\text{He}$  dilution refrigerator. The relaxation calorimeter is also used for measurements of the magnetic Grüneisen parameter.

**Dielectric measurements.** For measurements of the dielectric constant, a plate capacitor arrangement was realized by attaching two electrodes (silver paste) to opposite parallel surfaces of the samples. The dielectric constant was derived from the capacitance, read out by using an LCR meter (Agilent E4980), and the geometrical dimensions of the plate capacitor. Measurements were performed by using a top-loading  $^3\text{He}$ - $^4\text{He}$  dilution refrigerator.

**Ac-susceptibility.** For measurements the ac-susceptibility, a homemade susceptometer adapted to a top-loading  $^3\text{He}$ - $^4\text{He}$  dilution refrigerator was employed.

## References

- [1] Koteswararao, B. *et al.* Magnetic properties and heat capacity of the three-dimensional frustrated  $S = 1/2$  antiferromagnet  $\text{PbCuTe}_2\text{O}_6$ . *Phys. Rev. B* **90**, 035141 (2014).
- [2] Khuntia, P. *et al.* Spin Liquid State in the 3D Frustrated Antiferromagnet  $\text{PbCuTe}_2\text{O}_6$ : NMR and Muon Spin Relaxation Studies. *Phys. Rev. Lett.* **116**, 107203 (2016).
- [3] Chillal, S. *et al.* Evidence for a three-dimensional quantum spin liquid in  $\text{PbCuTe}_2\text{O}_6$ . *Nat. Commun.* **11**, 2348 (2020).
- [4] Balents, L. Spin liquids in frustrated magnets. *Nature* **464**, 199 (2010).
- [5] Lacroix, C., Mendels, P. and Mila, F. *Introduction to Frustrated Magnetism*. Springer Series in Solid-State Sciences Vol. **164** (Springer, New York, 2011).
- [6] Savary, L., Balents, L. Quantum spin liquids: A review. *Rep. Prog. Phys.* **80**, 016502 (2017).

- [7] Zhou, Y. Kanoda, K., Ng, T.-K. Quantum spin liquid states. *Rev. Mod. Phys.* **89**, 025003 (2017).
- [8] Broholm, C. *et al.* Quantum spin liquids. *Science* **367**, 263 (2020).
- [9] Helton, J. S. *et al.* Spin Dynamics of the Spin-1/2 Kagome Lattice Antiferromagnet  $\text{ZnCu}_3(\text{OH})_6\text{Cl}_2$ . *Phys. Rev. Lett.* **98**, 107204 (2007).
- [10] Han, T.-H. *et al.* Fractionalized excitations in the spin-liquid state of a kagome-lattice antiferromagnet. *Nature* **492**, 406 (2012).
- [11] Shimizu, Y., Miyagawa, K., Kanoda, K., Maesato, M., Saito, G. Spin Liquid State in an Organic Mott Insulator with a Triangular Lattice. *Phys. Rev. Lett.* **91**, 107001 (2003).
- [12] Itou, T., Oyamada, A., Maegawa, S., Tamura, M., Kato, R. Quantum spin liquid in the spin-1/2 triangular antiferromagnet  $\text{EtMe}_3\text{Sb}[\text{Pd}(\text{dmit})_2]_2$ . *Phys. Rev. B* **77**, 104413 (2008).

- [13] Powell, B. J., McKenzie, R. H. Quantum frustration in organic Mott insulators: From spin liquids to unconventional superconductors. *Rep. Prog. Phys.* **74**, 056501 (2011).
- [14] Gardner, J. S., Gingras, M. J. P., and Greedan, J. E. Magnetic pyrochlore oxides. *Rev. Mod. Phys.* **82**, 53 (2010).
- [15] Rau, J. G., Gingras, M. J. P., Frustrated quantum rare-earth pyrochlores. *Annu. Rev. Condens. Matter Phys.* **10**, 357 (2019).
- [16] Okamoto, Y., Nohara, M., Aruga-Katori, H., Takagi, H. Spin-Liquid State in the  $S = 1/2$  Hyperkagome Antiferromagnet  $\text{Na}_4\text{Ir}_3\text{O}_8$ . *Phys. Rev. Lett.* **99**, 137207 (2007).
- [17] Elhadj, M., Canals, B., Lacroix, C. Symmetry breaking due to Dzyaloshinsky-Moriya interactions in the kagome lattice. *Phys. Rev. B* **66**, 014422 (2002).
- [18] Cépas, O., Fong, C. M., Leung, P. W., Lhuillier, C. Quantum phase transition induced by Dzyaloshinskii-Moriya interactions in the kagome antiferromagnet. *Phys. Rev. B* **78**, 140405(R) (2008).

- [19] Chen, G., Balents, L. Spin-orbit effects in  $\text{Na}_4\text{Ir}_3\text{O}_8$ : A hyper-kagome lattice antiferromagnet. *Phys. Rev. B* **78**, 094403 (2008).
- [20] Singh, Y., Tokiwa, Y., Dong, J., Gegenwart, P. Spin liquid close to a quantum critical point in  $\text{Na}_4\text{Ir}_3\text{O}_8$ . *Phys. Rev. B* **88**, 220413(R) (2013).
- [21] Weil, M., Shirkhanlou, M., Stürzer, T., Phase Formation Studies of Lead(II) Copper(II) Oxotellurates: The Crystal Structures of Dimorphic  $\text{PbCuTeO}_5$ ,  $\text{PbCuTe}_2\text{O}_6$ , and  $[\text{Pb}_2\text{Cu}_2(\text{Te}_4\text{O}_{11})](\text{NO}_3)_2$ . *Zeitschr. f. anorg. und allg. Chemie* **645**, 347 (2019).
- [22] Koteswararao, B. *et al.* Observation of  $S = \frac{1}{2}$  quasi-1D magnetic and magneto-dielectric behavior in a cubic  $\text{SrCuTe}_2\text{O}_6$ . *J. Phys.: Condens. Matter* **27**, 426001 (2015).
- [23] Hanna, A. R. *et al.* Crystal growth and characterization of  $\text{PbCuTe}_2\text{O}_6$  single crystals, to be published.
- [24] Köppen, M. *et al.* Solitary Magnetic Excitations in the Low-Carrier Density, One-Dimensional  $S = 1/2$  Antiferromagnet  $\text{Yb}_4\text{As}_3$ . *Phys. Rev. Lett.* **82**, 4548 (1999).

- [25] Kittel, Ch. *Introduction to Solid State Physics* (New York: Wiley).
- [26] Lines, M. E., and Glass, A. M. *Principles and Application of Ferroelectrics and Related Materials* (Clarendon, 1977).
- [27] Gati, E. *et al.* Evidence for Electronically Driven Ferroelectricity in a Strongly Correlated Dimerized BEDT-TTF Molecular Conductor. *Phys. Rev. Lett.* **120**, 247601 (2018).
- [28] Lunkenheimer, P. *et al.* Multiferroicity in an organic charge-transfer salt that is suggestive of electric-dipole-driven magnetism. *Nature Materials* **11**, 755 (2012).
- [29] Zhong, W. L. *et al.* Phase transition in PbTiO<sub>3</sub> ultrafine particles of different sizes. *J. Phys.: Condens. Matter* **5**, 2619 (1993).
- [30] Chattopadhyay, S., Ayyub, P., Palkar, V. R., Multani, M. Size-induced diffuse phase transition in the nanocrystalline ferroelectric PbTiO<sub>3</sub>. *Phys. Rev. B* **52**, 13177 (1995).
- [31] Zhao, Z. *et al.* Grain-size effects on the ferroelectric behavior of dense nanocrystalline BaTiO<sub>3</sub> ceramics. *Phys. Rev. B* **70**, 024107 (2004).

- [32] Nakatsuji, S. *et al.* Spin Disorder on a Triangular Lattice. *Science* **309**, 1697 (2005).
- [33] Cheng, J.G. *et al.* High-Pressure Sequence of Ba<sub>3</sub>NiSb<sub>2</sub>O<sub>9</sub> Structural Phases: New  $S = 1$  Quantum Spin Liquids Based on Ni<sup>2+</sup>. *Phys. Rev. Lett.* **107**, 197204 (2011).
- [34] Zhu, L., Garst, M., Rosch, A., Si, Q. Universally Diverging Grüneisen Parameter and the Magnetocaloric Effect Close to Quantum Critical Points. *Phys. Rev. Lett.* **91**, 066404 (2003).
- [35] Wolf, B. *et al.* Magnetocaloric effect and magnetic cooling near a field-induced quantum-critical point. *Proc. Natl. Acad. Sci. USA* **108**, 6862 (2011).
- [36] Tokiwa, Y., Stingl, Ch., Kim, M.-S., Takabatake, T., Gegenwart, P. Characteristic signatures of quantum criticality driven by geometrical frustration. *Sci. Adv.* e1500001 (2015).
- [37] Tokiwa, Y., Ishikawa, J.J., Nakatsuji, S., Gegenwart, P. Quantum criticality in a metallic spin liquid. *Nature Materials* **13**, 356 (2014).

- [38] Matsumoto, Y. *et al.* Quantum Criticality Without Tuning in the Mixed Valence Compound  $\beta$ -YbAlB<sub>4</sub>. *Science* **331**, 316 (2011).
- [39] Pott, R., Schefzyk, R. Apparatus for measuring the thermal expansion of solids between 1.5 and 380 K. *J. Phys. E* **16**, 444 (1983).

### **Acknowledgements**

Work done at Goethe University Frankfurt was supported by the German Science Foundation (DFG) through the SFB/TR 288 (ID 422213477). B.L., A.H. and A.T.M.N. I. acknowledge the support of DFG through project B06 of SFB 1143 (ID 247310070). We acknowledge fruitful discussions with Christian Hess, Xiao-Chen Hong, Peter Lunkenheimer, Elena Gati and Harald O. Jeschke.

### **Author contributions**

B.L., S.C., B.W. and M.L. planned the project. Measurements and analysis of specific heat and magnetic Grüneisen parameter were performed by P.E. and U.T. Measurements and analysis of thermal expansion were performed by C.T., Y.S., S. H., B.W. and M.L. Measurements and analysis of the magnetic susceptibility were performed by B.W. and P.E. Measurements and analysis of the dielectric constant were performed by A.A. and U.T. Measurements and analysis of ultrasonic

experiments were performed by J.Z. and B.W. The samples were synthesized and characterized by A.H., S.C., A.T.M.N.I. and B.L. B.W. and M.L. discussed the results and prepared the manuscript.

### **Additional information**

Supplementary information is available in the online version of the paper. Correspondence and request for materials should be addressed to C.T.

### **Competing financial interests**

The authors declare no competing financial interests.